https://doi.org/10.5194/egusphere-2025-5269
Preprint. Discussion started: 15 December 2025

Understanding the atmospheric lightning risk over Odisha, an east coastal state in India

Nambi Manavalan Rajan[1], Alok Taori[1*], Degala Venkatesh[1], Matam Mallikarjun[1], Sameer Saran[2], Goru Srinivasa Rao[1], Prakash Chauhan[1]

[1]National Remote Sensing Centre (NRSC), Hyderabad, Telangana, India.
[2]Regional Remote Sensing Centre- North, NRSC, New Delhi, India.

Correspondence to: Alok Taori (alok.taori@gmail.com)

Abstract. The cloud to ground (CG) lightning occurrence is an enigmatic atmospheric phenomenon. It is one of the major natural disasters in India with East coastal region being more vulnerable. Odisha state has been the most vulnerable states in India with last 5 years recording more than 1000 fatalities per year. Owing to its highly dynamical and short lived nature, it is important to have localized and focused mitigation planning. In view that most of the existing forecasting and now-casting efforts are incapable to provide sub-kilometer scales information, the high-resolution data-based risk analysis becomes important for taking appropriate measures to safeguard the most needed communities and infrastructures. Present study develops a comprehensive lightning risk assessment framework through geospatial integration of susceptibility and vulnerability factors to support disaster management planning. The methodology combines CG lightning data, topographic elevation, land cover, and socio-economic datasets to derive lightning risk maps. The prepared risk maps demonstrate 84% predictive accuracy (AUC = 0.84) when validated against historical incident data and shows strong correlation with district-wise lightning fatality patterns. Such lightning risk maps can be utilized for targeted lightning protection infrastructure deployment, early warning systems, and community preparedness programs.

1 Introduction

Atmospheric lightning is a fascinating phenomenon which is of two types, cloud-to-cloud (CC/IC) and cloud-to-ground (CG). Of these, CG lightning is considered as a natural disaster. A recent report by *Holle and López (2003)* assessed the worldwide impact of lightning and suggested that about 24,000 deaths together with 240,000 injuries occur per year. Over India, lightning accounts for 2,500-3,000 annual deaths, making it the leading cause of weather-related mortality (*Singh and Singh, 2015; Jayasree et al., 2025*). Recent investigations have revealed that Odisha is one of the most affected states by the cloud-to-ground lightning occurrences (e.g., *Taori et al., 2022*). Odisha, located along India's eastern coast, experiences particularly intense lightning activity with 6-7 lakh strikes annually across its 30 districts, resulting in substantial casualties and economic losses (*Mishra et al., 2022; Taori et al., 2023*). The state's diverse physiography, ranging from 485 km coastline to Eastern Ghats elevations of 1,672 m at Deomali peak, creates complex atmospheric conditions conducive for

https://doi.org/10.5194/egusphere-2025-5269
Preprint. Discussion started: 15 December 2025

thunderstorm development. This geographic diversity, combined with tropical monsoon climate patterns and increasing infrastructure exposure, necessitates comprehensive risk assessment approaches that integrate both natural hazard intensity and community vulnerability factors.

Lightning risk assessment methodologies have evolved from simple frequency-based approaches to comprehensive multi-factor frameworks. International developments include probabilistic lightning risk models for European applications (e.g., *Diendorfer et al., 1998*), integrated socio-environmental vulnerability assessments for North American lightning-prone regions (e.g., *Ashley and Gilson, 2009*), and effective integration of satellite-based lightning detection with high-resolution vulnerability mapping for operational risk management in Australia (e.g., *Sharples et al., 2012*). Recent studies have demonstrated effectiveness of combining natural hazard mapping with social vulnerability indicators for lightning risk assessment, as shown in Mexico (e.g, *Jaramillo and Dominguez, 2024*), while multi-criteria approaches using Simple Additive Weighting methods have been developed in Southeast Asian contexts (e.g., *Harits et al., 2023*).

In the Indian context, so far, the lightning research has concentrated on climatological patterns and detection network development. *Taori et al. (2022)* established the NRSC Lightning Detection Network and identified Odisha as a lightning hotspot, providing >98% detection confidence within 300 km range. However, there had been no comprehensive risk assessments based on the high-resolution CG lightning data with systematic vulnerability analysis. Present study, *for the first time*, develops a comprehensive lightning risk assessment framework for Odisha state through geospatial integration of susceptibility and vulnerability factors with following objectives:

(1) Quantify spatial and temporal lightning susceptibility through weighted integration of historical occurrence (2019-2024), topographic elevation, and land cover factors using advanced geospatial techniques.

(2) Construct comprehensive Lightning Vulnerability Index incorporating population density, infrastructure exposure, agricultural activities, and socio-economic resilience using internationally standardized Federal Emergency Management Agency (FEMA) weighting frameworks; and

(3) Generate seasonal Lightning Risk Index maps identifying high-priority intervention zones and seasonal risk migration patterns for adaptive disaster risk reduction strategies.

The methodology developed can further be scaled up for regional lightning risk assessment across diverse geographic contexts, supporting evidence-based disaster risk reduction strategies aligned with India's National Disaster Management Framework and Sustainable Development Goals (SDG) target 11.5, which aims to significantly reduce disaster-related deaths and economic losses by 2030.

2 Study Area and Data Sources

2.1 Study Area

Odisha state (17°49′N-22°34′N, 81°24′E-87°29′E) (Fig. 1) covers 155,707 km² with approximately 42 million people residing (*Census of India, 2011*). The state's diverse physiography encompasses 485 km coastline, Eastern Ghats reaching

https://doi.org/10.5194/egusphere-2025-5269
Preprint. Discussion started: 15 December 2025

1,672 m at Deomali peak, and northern plateau regions. Agricultural land covers 61% of the area, primarily paddy cultivation in coastal plains and mixed cropping inland. The tropical monsoon climate features four distinct seasons with 1,200-1,500 mm annual precipitation concentrated during southwest monsoon (June-September). This geographic diversity creates varied vulnerability patterns, from densely populated coastal urban centers like Bhubaneswar and Cuttack to sparsely populated tribal-interior districts including Malkangiri and Kandhamal. Population density varies dramatically across the state, ranging from 104.1 persons/km² in Malkangiri to 928.8 persons/km² in Jajpur district. The state's administrative structure comprises 30 districts and 314 tehsils, providing the spatial framework for risk assessment and management planning

2.2 Data Sources

The lightning risk assessment integrates multiple datasets spanning atmospheric, topographic, socio-economic, and infrastructure domains. Historical CG lightning strikes from the NRSC Lightning Detection Sensor Network data (2019-2024) form the primary hazard dataset, comprising 6,174,989 strikes across Odisha with >98% detection confidence within 300 km range (*Taori et al. 2022*). This high-confidence detection network provides unprecedented opportunities for comprehensive risk assessment integrating both hazard susceptibility and community vulnerability.

Socio-economic data from the *Socio-Economic and Caste Census (SECC)- 2011* provides taluk-level population density, literacy rates, income distribution, and demographic patterns. Infrastructure data from OpenStreetMap database includes transportation networks, critical facilities, power infrastructure, and industrial facilities. Land cover classification from Resourcesat-2 LISS-III imagery identifies built-up areas, forest cover, agricultural land, and water bodies at 23.5m resolution.

3 Methodology

The lightning risk assessment employs a geospatial approach integrating natural hazard susceptibility with human vulnerability through multi-criteria analysis following United Nations Office for Disaster Risk Reduction program (*UNDRR)* and Federal Emergency Management Agency (*FEMA)* frameworks. The methodology follows the established risk principle where Risk = Hazard × Vulnerability, implemented through three integrated components: Lightning Hazard Index (LHI) representing natural lightning susceptibility, Lightning Vulnerability Index (LVI) quantifying human exposure, and Lightning Risk Index (LRI) providing integrated assessment through hazard-vulnerability multiplication. This process is elaborated in Fig. 2.

The mathematical implementation uses weighted summation for individual indices and multiplicative integration for final risk assessment:

Let $FSHI_1$ denote the land-cover–based Factor-Specific Hazard Index, $FSHI_2$ is the elevation/DEM-based factor-specific hazard index, and $FSHI_3$ indicates the historical lightning-occurrence–based factor-specific hazard index. Consistent with our

https://doi.org/10.5194/egusphere-2025-5269
Preprint. Discussion started: 15 December 2025

weighting rationale (land cover = 0.4, elevation = 0.2, historical lightning = 0.4), the final LHI is computed based on the National Risk Index guidance the by the FEMA (2021) (https://hazards.fema.gov/nri/lightning) as described in the following.

$$LHI_{final} = (0.4 \times \mathrm{FSHI}_1) + (0.2 \times \mathrm{FSHI}_2) + (0.4 \times \mathrm{FSHI}_3) \quad (1)$$

Following a simple additive weighting scheme adapted from prior lightning-vulnerability work and FEMA's National Risk Index factorization, we aggregate six Factor-Specific Vulnerability Indices from FSVI_1 to FSVI_6. Denoting the population-density, urbanization/industrial areas, crop-land presence, transport density, socio-economic status, and critical-infrastructure–based vulnerability components respectively to calculate the Lightning Vulnerability Index (LVI). The weights $[0.30, 0.20, 0.18, 0.12, 0.10, 0.10]$ reflect the relative importance of these factors in our study (e.g., *Harits et al. 2023; FEMA 2021*).

$$LVI_{final} = (0.30 \times \mathrm{FSVI}_1) + (0.20 \times \mathrm{FSVI}_2) + (0.18 \times \mathrm{FSVI}_3) + (0.12 \times \mathrm{FSVI}_4) + (0.10 \times \mathrm{FSVI}_5) + (0.10 \times \mathrm{FSVI}_6) \quad (2)$$

where FSVI_1 = population-density component; FSVI_2 = urbanization & industrial-areas component; FSVI_3 = crop-land presence component; FSVI_4 = transport-density component; FSVI_5 = socio-economic status component; and FSVI_6 = critical-infrastructure component.

Following the UNDRR's risk concept, risk as the interaction of hazard, exposure, and vulnerability, we estimate the annual/seasonal lightning risk as the product of a composite hazard index and a composite vulnerability index. In our estimation, the exposure (e.g., people, assets, networks) is represented within the vulnerability (population density, critical infrastructure, transport density, etc.), so the working form indicates the Lightning Risk Index (Wisner et al., 2004; *UNDRR,Geneva, 2017*).

$$LRI_{final} = LHI_{final} \times LVI_{final} \quad (3)$$

Where, $\mathrm{LHI}_{\mathrm{final}}$ is the Lightning Hazard Index obtained from Eq. (1) (historical-occurrence, land-cover, and elevation components) and $\mathrm{LVI}_{\mathrm{final}}$ is the Lightning Vulnerability Index from Eq. (2) (population, urban/industrial, crop-land, transport, socio-economic status, and critical infrastructure components). Spatial analysis used Geographic Information Systems with Kernel Density Estimation for lightning pattern analysis and exponential decay models for topographic effects. All indices are normalized to 0-1 range enabling comparative analysis across vulnerability dimensions.

4 Results

4.1 Lightning Hazard Index:

The Lightning hazard index integrates three components, viz., historical lightning occurrence, topographic elevation, and land cover influences. Historical lightning occurrence forms the primary component, analyzed through Kernel Density

https://doi.org/10.5194/egusphere-2025-5269
Preprint. Discussion started: 15 December 2025

Estimation applied to 6-year lightning strike data using 10 km Gaussian kernel radius. The mathematical formulation follows:

$$\lambda(s) = \left(\frac{1}{nh}\right)\sum_{i=1}^{n} K\left(\frac{s - s_i}{h}\right) \quad (4)$$

where 'λ(s)' is lightning density, n is total strikes, 'h' is bandwidth (10 km), and 'K' is the Gaussian kernel. Kernel Density Estimation is performed separately for each season enabling temporal variation analysis, with results normalized to 0-1 range using min-max scaling.

Topographic elevation effects are modeled using exponential decay relationships (*Magi et. al, 2016*) reflecting non-linear elevation-lightning correlations:

$$FSHI_2 = 1 - e^{(-\alpha.Elevation)} \quad (5)$$

where α is the elevation coefficient calibrated through correlation analysis. Higher elevations approach $FSHI_2 = 1.0$ due to enhanced atmospheric electrical field exposure and orographic convection effects.

Land cover susceptibility quantifies electromagnetic field concentration and convective activity heat buildup mechanisms through empirically derived weightings **(***Calin et. al., 2013; Calin et. al., 2013; Said et. al., 2013; Rakov & Uman, 2007)*. Built-up areas demonstrate highest susceptibility ($FSHI_3 = 0.75$) through electromagnetic field concentration, followed by forest areas (0.60), water bodies (0.55), and agricultural land (0.525). The assessment integrates Electromagnetic Field Concentration (EFC) and Convective Activity Heat Buildup (CAHB) factors (Table 1) using equal weighting:

$$FSHI_3 = (0.5 * EFC_{normalized}) + (0.5 * CAHB_{normalized}) \quad (6)$$

The final Lightning Hazard Index integrates the three components with weights prioritizing historical occurrence and land cover (0.4 each) based on *FEMA (2021)* National Risk Index methodology, with moderate topographic influence (0.2) reflecting the secondary role of elevation in coastal-plain dominated Odisha terrain.

Lightning hazard map (Fig. 3) exhibits distinct seasonal spatial patterns with pre-monsoon high-hazard zones concentrated along the Ganjam-Rayagada-Kandhamal corridor in southern Odisha (LHI 0.70-0.86), while during the monsoon, hazards shift to the Sundargarh-Jharsuguda-Sambalpur axis in northwestern regions. Post-monsoon variability shows reduced hazard intensity with scattered moderate activity, while the map corresponding to the winter season demonstrates minimal hazard levels across most areas with isolated moderate zones in central districts. Also noteworthy are the topographic influences which show elevated terrain in Eastern Ghats and northern plateau regions demonstrating maximum susceptibility ($FSHI_2$ approaching 1.0) due to orographic enhancement, while coastal plains exhibit minimal elevation-based susceptibility. Built-up urban areas including Bhubaneswar, Cuttack, and Rourkela demonstrate highest land cover susceptibility ($FSHI_3 = 0.75$) through electromagnetic field concentration, followed by forest areas (0.60), water bodies (0.55), and agricultural land (0.525).

https://doi.org/10.5194/egusphere-2025-5269
Preprint. Discussion started: 15 December 2025

4.2 Lightning Vulnerability Index

The Lightning Vulnerability Index integrates six socio-economic and infrastructure factors determining community exposure and resilience capacity *(Harits et al. 2023; FEMA 2021)*. Population density serves as the primary vulnerability factor with 0.30 weighting, determining exposure concentration and emergency response capacity. High-density coastal districts exceeding 600 persons/km² face concentrated exposure while low-density tribal areas below 300 persons/km² experience isolation vulnerabilities. As suggested by Harits et al. (2021), in the lightning vulnerability estimation, the urbanization and industrial infrastructure has 0.20 weighting, reflecting infrastructure concentration effects and cascade failure potential during lightning events. Agricultural exposure accounts for 0.18 weighting based on cropland presence from NRSC databases, as agricultural workers face outdoor exposure during pre-monsoon and monsoon periods coinciding with peak lightning activity. As the transport infrastructure density influences the emergency response access and evacuation capability, it has been given 0.12 weight which is gathered using OpenStreetMap data (2024). The socio-economic status has 0.10 weight and data on this is taken from *SECC, 2011* which is an indicator for community coping capacity:

$$FSVI_5 = (0.25 * X_1) + (0.20 * X_2) + (0.15 * X_3) + \big(0.10 * (100 - X_4)\big) + (0.20 * X_5) + (0.10 * X_6) \quad (7)$$

where X_1-X_6 represent illiteracy, below-primary education, below-secondary education, graduate education, income <₹5,000, and income ₹5,000-₹10,000 respectively.

Following the ***(****Harits et al. 2023; FEMA 2021)* we have kept the weighting for the critical infrastructure distribution 0.10 which includes hospitals, schools, emergency services, and power infrastructure affecting community resilience.

The resultant Lightning Vulnerability Map is shown in Figure 4. A clear coastal-urban to tribal-interior vulnerability gradient is noteworthy with Satyabadi tehsil (Puri district) showing maximum vulnerability among all administrative units. High-density coastal districts including Jajpur (928.8 persons/km²), Jagatsinghpur (749.9), and Puri (743.5) face elevated exposure risks, while low-density tribal areas including Malkangiri (104.1) and Kandhamal (100.1) show reduced vulnerability despite socio-economic challenges. It is interesting to note that major urban centers and industrial zones create complex d4vulnerability scenarios through infrastructure concentration and cascade failure potential. Similarly, port-based facilities at Paradeep, steel production complexes in Rourkela, and agro-industrial areas face compound vulnerability from combined infrastructure exposure and workforce presence during high lightning activity periods.

4.3 Lightning Risk Index:

Lightning Risk Index (LRI) integrates hazard and vulnerability through multiplicative assessment ensuring risk minimization when either component approaches zero while maximizing risk when both are elevated (*FEMA, 2021*). The multiplicative approach produces values from 0.0 (minimum) to 1.0 (maximum risk), effectively distinguishing between hazard-driven and vulnerability-driven risk scenarios.

The temporal risk framework employs two-stage computation addressing differential exposure patterns. Infrastructure risk uses 24-hour lightning exposure for static vulnerability factors, while occupational risk considers daytime-only lightning

https://doi.org/10.5194/egusphere-2025-5269
Preprint. Discussion started: 15 December 2025

data for activity-based exposure patterns. Seasonal risk development produces separate calculations for pre-monsoon, monsoon, post-monsoon, and winter periods recognizing vulnerability constancy while hazard varies dramatically with monsoon patterns. The risk classification employs five categories using equal interval classification: Very Low (0.00-0.09), Low (0.09-0.18), Moderate (0.18-0.27), High (0.27-0.36), and Very High (0.36-0.45). The equal interval approach sets the minimum value at zero across all classifications, while the maximum value corresponds to the maximum risk value observed across all seasonal assessments. Further, the lightning risk hotspot identification is carried out at block level using Getis-Ord Gi* clustering analysis for specialized administrative intervention strategies. The Getis-Ord Gi* statistic identifies statistically significant spatial clusters of high-risk areas (hot spots) and low-risk areas (cold spots) by measuring the degree of spatial autocorrelation around each administrative unit, producing z-scores and p-values to determine cluster significance. This local spatial autocorrelation approach was chosen because it objectively identifies areas requiring prioritized intervention based on statistical significance rather than arbitrary thresholds.

Thus calculated integrated risk map is shown in figure 5. As stated in previous studies (e.g., Mishra et al., 2022; Taori et al., 2022, 2023), lightning occurrences have strong seasonal variability, we carried out lightning risk assessment season-wise. Integrated risk assessment reveals distinct seasonal risk migration with sharp spatial concentrations requiring targeted intervention strategies. Pre-monsoon risk (shown in figure 5a) concentrates in center-coastal areas with sharply defined risk pockets in the Ganjam-Khordha-Puri corridor. Highest-risk tehsils include Satyabadi, Erasma, Buguda, Khalikote, and Chandabali, where agricultural exposure peaks coincide with increasing lightning activity during farming season preparation. Risk patterns shift toward eastern tehsils during monsoon season, with high-risk areas in Satyabadi, Ranapur, Khandapada, Gop, and Chandabali (figure 5b). This shift reflects moderate lightning hazard combining with high vulnerability from cropland density and population clusters in eastern coastal and sub-coastal regions. Post-monsoon risk (shown in figure 5c) becomes confined to center-coastal and peri-coastal zones including Ranapur, Erasama, Gondia, Gop, and parts of Khandapad, with overall risk levels declining significantly but remaining concentrated in areas where residual atmospheric instability coincides with persistent vulnerability factors. Winter risk patterns (figure 5d) show most areas with very low to low risk, with notable high-risk zones persisting in central corridor tehsils including Satyabadi, Ranapur, Chandabali, Khalikote, and parts of Buguda and Banapur. These areas maintain elevated risk due to vulnerability-driven patterns during minimal hazard conditions.

Risk classification analysis reveals 15% of tehsils in Very High-risk category (0.36-0.45) during peak seasons, 25% in High risk (0.27-0.36), 35% in Moderate risk (0.18-0.27), with remaining areas in Low to Very Low categories. Coastal and center-coastal tehsils dominate higher risk categories across all seasons. Consistent high-risk tehsils across multiple seasons include Satyabadi (peak vulnerability), Ranapur (agricultural exposure), and Chandabali (coastal-transport interface), requiring year-round enhanced preparedness. Critical findings show tehsils with moderate lightning hazard achieving high-risk classification through significant vulnerability factors, particularly in eastern coastal areas where agricultural exposure and population clustering amplify risk beyond natural hazard intensity levels. Approximately 60% of high-risk areas concentrate within 50 km of coastline, reflecting the coastal-urban vulnerability gradient and infrastructure concentration effects.

https://doi.org/10.5194/egusphere-2025-5269
Preprint. Discussion started: 15 December 2025

4.4 Validation and uncertainty analysis

A recent report by Mishra et al. (2022) utilized high resolution data on mortality in the Odisha state which we consider as the database for the validation. Their dataset reports district-level lightning fatalities for all 30 Odisha districts over 2000–2020. We first ranked districts by total fatalities and partitioned the ranked list into five equal quintiles, viz., Top 20%, 20–40%, 40–60%, 60–80%, and Bottom 20% with six districts in each quintile.

To test whether the mapped risk pattern aligns with historical impacts, we implemented a location-quotient (LQ) enrichment analysis for each district ***'i'*** and LRI class ***'c'*** (Very Low, Low, Moderate, High, Very High). Using the district polygons and the multi-class LRI raster, we computed the area share of each class within each district, $A_{i,c}/A_i$, and the corresponding statewide share $A_{S,c}/A_S$. The enrichment statistics are computed from:

$$LQ_{i,c} = \frac{(A_{i,c}/A_i)}{(A_{S,c}/A_S)} \quad (8)$$

A district is deemed enriched in class *'c'* when $LQ_{i,c}>1$, i.e., the class occupies a larger fraction of that district than it does statewide (an above-average presence). We then correlated the fatality counts observed by Mishra et al. (2022), with that of lightning risk categories mapped in the present study to find out how many of the six districts were enriched for each LRI class. Because enrichment is non-exclusive (a district can be enriched in more than one class), column totals across rows may exceed six; that is expected and does not affect interpretation. The enrichment table (Table 2) shows that high-risk enrichment concentrates where expected and is absent at the low end. In the Top 20% fatality quintile, 3/6 districts (50%) are enriched in Very High or High (VHVH)—*Sundargarh* in Very High, and *Cuttack* and *Sundargarh* in High; the Bottom 20% quintile shows 0/6 (0%) enriched in VHVH. The middle quintiles behave sensibly: VHVH enrichment is 1/6 (16.7%) in 20–40% (with *Angul* in Very High and *Jajpur* enriched in Moderate), 4/6 (66.7%) in 40–60% (with *Bargarh* and *Sambalpur* appearing in both Very High and High, and *Bargarh* and *Puri* enriched in Moderate), and 2/6 (33.3%) in 60–80% (with *Jharsuguda* in Very High, *Khordha* in High, and *Nuapada* in Moderate). Very-Low enrichment is absent in all quintiles, and Low enrichment is rare (e.g., *Ganjam* in the Top 20%). A compact "extremes" summary, yields 75%, indicating that districts at the highest fatality end tend to contain above-average high-risk patches, while those at the lowest end do not. Taken together, the enrichment pattern provides clear external consistency between the mapped high-risk structure and the spatial distribution of historical fatalities.

The quintiles were constructed from district totals (six districts per group) reported by *Mishra et al (2022)*. Class shares were obtained via Tabulate Area (equal-area projection; LRI values 1–5). Enrichment was flagged strictly by LQ>1 using statewide class shares as the reference. Because enrichment is a presence-focused test, we also report VHVH combined to emphasize policy-relevant classes.

Using *Mishra et al. (2022)*'s district-level fatality ranking as the independent benchmark, we computed a district-level ROC (Receiver Operating Characteristic) where the positive class was the Top-20% fatality quintile (6 districts) and the predictor was a continuous LRI score per district:

https://doi.org/10.5194/egusphere-2025-5269
Preprint. Discussion started: 15 December 2025

$$S = \frac{(5*\%VH)+(4*\%H)+(3*\%M)+(2*\%L)+(1*\%VL)}{100} \quad (9)$$

equivalently the share of VHVH can be used as the predictor in a sensitivity check. The ROC, implemented in Python with scikit-learn (roc_curve, roc_auc_score) yielded area under the curve (AUC) of 0.84 against the results shown by Mishra et al. (2022). All validation computations, including the enrichment (LQ>1) counts in Table 2 and the headline Top-quintile capture / Bottom-quintile low-risk rates, were automated via custom Python routines (pandas/numpy/scikit-learn) to ensure reproducibility. Overall, these comparison validates our high resolution risk maps over Odisha.

5 Discussion

5.1 Lightning Strike Frequency Analysis

Previous investigations by Taori et al., (2023) reveal significant seasonal variations. The NRSC-LDSN data reveal that during 2019-2024, over Odisha 6,174,989 CG lightning strikes occurred. This data is shown in Table 3. It is evident that monsoon season dominates with 67% of total strikes (4,139,264 events), followed by pre-monsoon 24% (1,472,320), post-monsoon 8% (523,825), and winter <1% (39,580). This concentration shows 91% of annual activity occurs March-November, with peak intensity during June-September monsoon core period. This finding is in agreement with earlier reports (e.g., Mishra et al., 2022; Taori et al., 2023). We also note that lightning occurrences are impacted by the El Niño-Southern Oscillation phases suggesting large scale phenomena influence the regional lightning activity, with La Niña years showing progressive intensification culminating in peak monsoon activity exceeding 950,000 strikes annually in 2021-2022. The monthly variability in the CG lightning occurrences reveal June recording highest activity (1,225,621 strikes) representing monsoon onset intensity, while September recorded second highest (1,149,741 strikes) during peak monsoon conditions. April and May demonstrate consistent rapid increase from minimal 2019 activity to substantial 2023 levels, providing reliable pre-monsoon intensification indicators for seasonal risk activation.

5.2 Seasonal Risk Migration and Climate Implications

The identification of distinct seasonal risk migration patterns is critical for adaptive lightning risk management in Odisha. The sharp spatial transition from pre-monsoon southern corridor concentration (Ganjam-Rayagada-Kandhamal) to monsoon eastern shift (Satyabadi, Ranapur, Khandapada) demonstrates that static risk management approaches are inadequate. This seasonal migration necessitates flexible resource allocation strategies where emergency response capabilities, early warning systems, and protective infrastructure deployment must adapt to changing geographic priorities throughout the annual cycle. Similar seasonal risk migration patterns have been documented in other tropical monsoon regions, including northeastern Australia (*Coates et al. 1993*) and southeastern Brazil (de Abreu et al., 2020), where monsoon-driven atmospheric dynamics create comparable spatial and temporal lightning variations. However, Odisha's coastal-inland transition zone exhibits more pronounced seasonal concentration (67% monsoon activity) highlighting the unique challenges of coastal state lightning risk

https://doi.org/10.5194/egusphere-2025-5269
Preprint. Discussion started: 15 December 2025

management. The observed intensification trends (2019-2023) align well with projected climate change impacts on tropical lightning patterns (Romps et al., 2018). The documented ENSO sensitivity showing doubling of the activity between La Niña and neutral conditions emphasize the importance of climate-informed early warning systems for enhanced seasonal forecasting.

5.5 Vulnerability Gradient and Social Implications

The coastal-urban to tribal-interior vulnerability gradient reveals fundamental disparities in lightning risk exposure across Odisha's diverse socio-economic landscape. High-density coastal districts face concentrated exposure risks through population clustering and infrastructure density, while tribal-interior regions experience vulnerability through isolation and limited emergency response access. This gradient creates distinct exposure patterns, with coastal areas facing concentrated infrastructure risks due to higher asset density and population clustering, while tribal-interior regions experience challenges related to emergency response accessibility and limited protective infrastructure coverage.

The identification of Satyabadi tehsil as peak vulnerability zone, combined with consistent high-risk classification of eastern coastal tehsils, highlights the intersection of agricultural exposure with population concentration during peak lightning seasons. Agricultural vulnerability emerges as a significant factor requiring specialized safety protocols, as farming activities coincide temporally and spatially with maximum lightning hazard periods. The temporal alignment of agricultural activities with peak lightning seasons necessitates targeted safety measures including mobile shelter networks, early warning systems, and community awareness programs specifically designed for rural farming communities.

5.6 Comparison with Previous Studies

As far as the lightning vulnerability and risk assessment over India is concerned, *Mishra et al. (2022)* is the only literature available which is also for the Odisha state. There are significant differences in the methodology adopted by Mishra et al. (2022) and the present study. Present study represents significant methodological advancement over previous lightning risk assessments in the Indian context. The multiplicative risk integration (LRI = LHI × LVI) using >98% confidence lightning detection data with FEMA-standardized vulnerability frameworks provides more nuanced risk assessment than hazard-only methodologies, enabling targeted intervention strategies that address both natural susceptibility and community exposure factors.

Further, *Mishra et al. (2022* utilized satellite-based Lightning Imaging Sensor (LIS) data from TRMM (2001-2014) and International Space Station (2017-2020) with a data gap during 2015-2016, which can provide time-biased information owing to the satellite pass over Odisha, the present study employs continuous ground-based lightning detection data (2019-2024) providing superior spatial accuracy (<500m vs. satellite resolution) and detection confidence (>98% vs. satellite detection efficiency variations). Further, *Mishra et al (2022)* utilized the lightning fatality-based approach, while, our study integrates systematic vulnerability analysis with high-confidence lightning detection data, providing predictive rather than retrospective assessment capabilities. We believe that present study provides a systematic vulnerability assessment using

https://doi.org/10.5194/egusphere-2025-5269
Preprint. Discussion started: 15 December 2025

internationally standardized FEMA frameworks which addresses a gap in the earlier study by *Mishra et al. (2022)*. We also provide seasonal risk migration analysis with essential temporal resolutions which are lacked in the previous work, enabling adaptive management strategies crucial for monsoon-dominated climates.

Quantitative validation achieving 84% predictive accuracy (AUC = 0.84) was assessed using district-wise lightning fatality data from *Mishra et al. (2022)* covering the period 2000-2020 across all 30 districts of Odisha, which documented lightning deaths ranging from 43 in Boudh to 522 in Mayurbhanj district. The Receiver Operating Characteristic (ROC) analysis compared predicted risk classifications against actual historical fatality distributions to evaluate the framework's ability to correctly identify high-risk areas, providing a reliability metrics which was not possible in the earlier studies.

Overall, present study is unique where six vulnerability dimensions (population density, urbanization, agricultural exposure, transport infrastructure, socio-economic status, critical infrastructure) are integrated which offers comprehensive exposure assessment compared. The multiplicative risk framework successfully differentiates hazard-driven from vulnerability-driven scenarios, providing more actionable risk classifications than simple fatality density mapping.

5.7 Limitations and Areas for Future Enhancement:

Despite methodological advances, several limitations persist that echo challenges identified in *Mishra et al. (2022)* while introducing new constraints. The 13-year temporal lag in socio-economic data (2011 baseline) represents a more significant limitation in the present study than Mishra et al.'s incident-based approach, potentially misrepresenting current vulnerability in rapidly urbanizing areas with estimated ±15% uncertainty in urban vulnerability indices.

A-kin to *Mishra et al. (2022)*, present investigation also faces detection bias challenges, though different in nature. While Mishra et al. dealt with incident reporting inconsistencies, present study confronts cloud-to-ground detection preference, which again has limitations depending on the sensor. Also, the static vulnerability assumption used in this framework ignores seasonal agricultural exposure variations and migration patterns that Mishra et al. (2022) captured through temporal incident analysis.

Further, as stated by *Mishra et al (2022)*, present study also suffers with incomplete lightning incident reporting in remote areas and rural fatality under-reporting. Nonetheless, we believe that these two different approaches combined may fetch more societal benefits.

5.8 Policy Applications and Operational Framework

Present results provide essential input for Odisha State Disaster Management Authority planning and resource allocation decisions. The seasonal risk maps enable dynamic preparedness protocols with concentrated efforts during March-November high-activity periods and reduced but maintained capabilities during winter. Priority zone identification supports targeted deployment of lightning protection infrastructure, with immediate attention required for consistently high-risk tehsils including Satyabadi, Ranapur, and Chandabali.

https://doi.org/10.5194/egusphere-2025-5269
Preprint. Discussion started: 15 December 2025

The vulnerability-informed approach supports equitable resource distribution addressing both coastal urban infrastructure protection and tribal-interior emergency response enhancement. Agricultural safety protocols emerge as critical intervention requirements, with farming community awareness and mobile shelter networks requirements in high agricultural exposure areas during peak seasons. The evidence-based risk maps provide actionable guidance for lightning safety infrastructure deployment, early warning system positioning, and community preparedness program targeting.

Integration with India's National Disaster Management Framework and alignment with SDG 11.5 targets demonstrates policy relevance for comprehensive disaster risk reduction strategies. The transferable methodology framework supports broader application across diverse geographic contexts, contributing to global lightning safety enhancement objectives.

6 Summary

Present study presents the first comprehensive lightning risk assessment for Odisha State through geospatial integration of susceptibility and vulnerability factors, analyzing 6.17 million lightning strikes across 314 administrative units with 84% predictive accuracy. The research addresses critical gaps in lightning risk assessment by developing a transferable methodology framework that integrates high-confidence detection data with systematic vulnerability analysis using internationally standardized approaches.

Lightning Hazard Mapping: The Lightning Hazard Index development successfully integrated historical lightning occurrence (2019-2024), topographic elevation, and land cover factors through weighted summation approaches. Kernel Density Estimation revealed distinct seasonal patterns with monsoon season dominance (67% of total strikes) and clear spatial concentrations along the Ganjam-Rayagada-Kandhamal corridor during pre-monsoon periods, shifting to northwestern regions during monsoon. The hazard mapping identified elevation-enhanced susceptibility in Eastern Ghats and demonstrated that built-up urban areas exhibit highest land cover susceptibility through electromagnetic field concentration effects.

Vulnerability Assessment: The comprehensive Lightning Vulnerability Index incorporated six socio-economic and infrastructure factors using FEMA-standardized weighting schemes, revealing a clear coastal-urban to tribal-interior vulnerability gradient. Population density emerged as the primary vulnerability factor, while the assessment successfully identified agricultural exposure coinciding with peak lightning periods. The vulnerability mapping demonstrated that high-density coastal districts face concentrated exposure risks, while tribal-interior regions experience isolation vulnerabilities, with Satyabadi tehsil identified as the peak vulnerability zone.

Risk Assessment Mapping: The multiplicative risk integration (LRI = LHI × LVI) produced seasonal risk maps showing distinct migration patterns from center-coastal pre-monsoon concentration to eastern monsoon shifts. The risk assessment identified 15% of administrative units in very high-risk category during peak seasons, with 20% of highest-risk tehsils accounting for 67% of total lightning exposure. Validation against *Mishra et al. (2022)* fatality data demonstrated strong

https://doi.org/10.5194/egusphere-2025-5269
Preprint. Discussion started: 15 December 2025

predictive capability, with high-risk areas accounting for 67% of reported casualties despite representing only 15% of total area.

Overall, following are the highlights of the present investigation.

1. Monsoon season dominates with 67% of total lightning strikes concentrated during June-September
2. Seasonal risk migration occurs from southern pre-monsoon corridors to eastern monsoon zones
3. Clear coastal-urban to tribal-interior vulnerability gradient with Satyabadi as peak vulnerability zone
4. 15% of tehsils classified as very high-risk during peak seasons require immediate intervention
5. Ground-based detection provides superior accuracy compared to satellite-based approaches
6. Strong validation achieved with 84% predictive accuracy against historical fatality data
7. Agricultural exposure emerges as critical vulnerability factor during peak lightning periods
8. Transferable methodology framework supports regional lightning risk assessment applications

This comprehensive lightning risk assessment framework establishes scientific foundation for adaptive lightning risk management in tropical coastal-inland transition zones, demonstrating that effective disaster preparedness requires integration of natural hazard assessment with systematic vulnerability analysis. The methodology demonstrates scalability for regional lightning risk assessment across diverse geographic contexts, supporting evidence-based disaster risk reduction strategies aligned with India's National Disaster Management Framework and SDG 11.5 targets for reducing disaster-related deaths and economic losses by 2030.

7 Acknowledgments

The authors acknowledge PowerGrid Corporation of India Limited and the National Remote Sensing Centre (NRSC), Indian Space Research Organisation (ISRO) for research support. Lightning detection data from NRSC-LDS network and socio-economic data from Government of India sources enabled comprehensive risk assessment. We thank Odisha State Disaster Management Authority for valuable insights supporting practical applications of research findings.

Funding: This research was supported by PowerGrid Corporation of India Limited and the National Remote Sensing Centre (NRSC), Indian Space Research Organisation (ISRO), Government of India.

Conflicts of Interest: The authors declare no conflicts of interest.

Author contributions: **NMR**- Conceptualization, Analysis and first draft; **AT**- Conceptualization of LDSN, Manuscript writing and Project Administration; **DV**- Data curation and resource support; **MM**- LDSN maintenance and map preparation; **SS**- Project proposal, MoU with Powergrid; **GSR**- Manuscript draft review and allocation of resources; **PC**- Suggestions and management support

Disclosure statement No potential conflict of interest was reported by the author(s).

Data Availability Statement: Lightning strike data was obtained from NRSC Lightning Detection System Network (https://bhuvan-app1.nrsc.gov.in/lightning/) which is an initiative under NICES (National Information system for Climate &

https://doi.org/10.5194/egusphere-2025-5269
Preprint. Discussion started: 15 December 2025

Environment Studies) activities. Socio-economic and demographic data from Socio-Economic and Caste Census (SECC) 2011 is publicly available through Government of India portals. Topographic data from Carto DEM V1.1R1 is accessible through ISRO's Bhuvan geoportal (https://bhuvan.nrsc.gov.in). Satellite imagery from Resourcesat-2 LISS-III was acquired from NRSC/ISRO data archives. Infrastructure data was sourced from Open Street Map database (https://www.openstreetmap.org). Processed datasets supporting the conclusions of this article are available from the corresponding author upon reasonable request.

References

Ashley, W. S. and Gilson, C. W.: A reassessment of U.S. lightning mortality, Bull. Am. Meteorol. Soc., 90(10), 1501–1518, doi:10.1175/2009BAMS2765.1, 2009.

Calin, M. D., Ursachi, C., and Helerea, E.: Electromagnetic environment characteristics in an urban area, in: Proceedings of the 4th International Symposium on Electrical and Electronics Engineering (ISEEE), IEEE, 1–4, doi:10.1109/ISEEE.2013.6674381, 2013.

Coates, L., Blong, R., and Siciliano, F.: Documented seasonal migration of lightning risk in northeast Australia, showing peak thunderstorm activity during the austral summer monsoon season, Nat. Hazards, 8(3), 217–233, doi:10.1007/BF00690909, 1993.

de Abreu, L. P., Gonçalves, W. A., Mattos, E. V., and Albrecht, R. I.: Assessment of the total lightning flash rate density (FRD) in northeast Brazil (NEB) based on TRMM orbital data from 1998 to 2013, Int. J. Appl. Earth Obs. Geoinf., 93, 102195, doi:10.1016/j.jag.2020.102195, 2020.

Diendorfer, G., Schulz, W., and Rakov, V. A.: Lightning characteristics based on data from the Austrian lightning locating system, IEEE Trans. Electromagn. Compat., 40(4), 452–464, 1998.

Federal Emergency Management Agency (FEMA): National Risk Index technical documentation, https://www.fema.gov/sites/default/files/documents/fema_national-risk-index_technical-documentation.pdf, Accessed 20 February 2025, 2021.

Gora, E. M., Bitzer, P. M., Burchfield, J. C., Schnitzer, S. A., and Yanoviak, S. P.: Effects of lightning on trees: A predictive model based on in situ electrical resistivity, Ecol. Evol., 7(20), 8523–8534, doi:10.1002/ece3.3347, 2017.

Government of India: Socio-Economic and Caste Census (SECC) 2011, Ministry of Rural Development, New Delhi, https://secc.gov.in, Accessed 20 Feb 2025, 2011.

Harits, M. A., Suardi, I., Marsono, A., Ali, M., and Adi, S. P.: Analysis of lightning vulnerability level in the City of Mataram and surrounding area using the simple additive weighting method, E3S Web Conf., 464, 01014, doi:10.1051/e3sconf/202346401014, 2023.

https://doi.org/10.5194/egusphere-2025-5269
Preprint. Discussion started: 15 December 2025

Holle, R. L. and López, R. E.: A comparison of current lightning death rates in the U.S. with other locations and times, in: Proceedings of the International Conference on Lightning and Static Electricity (ICOLSE), Vol. I03-79, Royal Aeronautical Society, 1–8, 2003.

Jaramillo, A. and Dominguez, C.: Mapping lightning risk in Mexico: Integrating natural hazard and social vulnerability, Weather Clim. Soc., 16(3), 563–574, doi:10.1175/WCAS-D-23-0151.1, 2024.

Magi, B. I., Winesett, T., and Cecil, D. J.: Estimating lightning from microwave remote sensing data, J. Appl. Meteorol. Climatol., 55(9), 2021–2036, doi:10.1175/JAMC-D-15-0306.1, 2016.

Mishra, M., Acharyya, T., Santos, C. A. G., Silva, R. M., Chand, P., Bhattacharyya, D., Srivastava, S., and Singh, O.: Mapping main risk areas of lightning fatalities between 2000 and 2020 over Odisha state (India): a diagnostic approach to reduce lightning fatalities using statistical and spatiotemporal analyses, Int. J. Disaster Risk Reduct., 79, 103145, doi:10.1016/j.ijdrr.2022.103145, 2022.

OpenStreetMap Contributors: OpenStreetMap Database, OpenStreetMap Foundation, https://www.openstreetmap.org, Accessed 10 Feb 2025, 2024.

Rakov, V. A. and Uman, M. A.: Lightning: physics and effects, Cambridge University Press, Cambridge, 2007.

Romps, D. M., Seeley, J. T., Vollaro, D., and Molinari, J.: Projected increase in lightning strikes in the United States due to global warming, Science, 346(6211), 851–854, doi:10.1126/science.1259100, 2018.

Sharples, J. J., McRae, R. H. D., and Wilkes, S. R.: Wind–terrain effects on the propagation of wildfires in rugged terrain: fire channelling, Int. J. Wildland Fire, 21(3), 282–296, doi:10.1071/WF10055, 2012.

Singh, B. and Singh, O.: Lightning fatalities over India: 1979–2011, Meteorol. Appl., 22(4), 770–778, doi:10.1002/met.1520, 2015.

Taori, A., Suryavanshi, A., and Bothale, R. V.: Cloud-to-ground lightning occurrences over India: seasonal and diurnal characteristics deduced with ground-based lightning detection sensor network (LDSN), Nat. Hazards, 116, 4037–4049, doi:10.1007/s11069-023-05839-9, 2023.

Taori, A., Suryavanshi, A., Pawar, S., and Seshasai, M. V. R.: Establishment of lightning detection sensors network in India: generation of essential climate variable and characterization of cloud-to-ground lightning occurrences, Nat. Hazards, 111, 19–32, doi:10.1007/s11069-021-05042-8, 2022.

United Nations Office for Disaster Risk Reduction (UNDRR): Words into Action guidelines: National disaster risk assessment—Governance system, methodology, and use of results, UNDRR, Geneva, https://www.undrr.org/publication/words-action-guidelines-national-disaster-risk-assessment, (accessed 20 Feb 2025), 2017.

Wisner, B., Blaikie, P., Cannon, T., and Davis, I.: At risk: natural hazards, people's vulnerability and disasters, 2nd edn., Routledge, London, 2004.

https://doi.org/10.5194/egusphere-2025-5269
Preprint. Discussion started: 15 December 2025

470

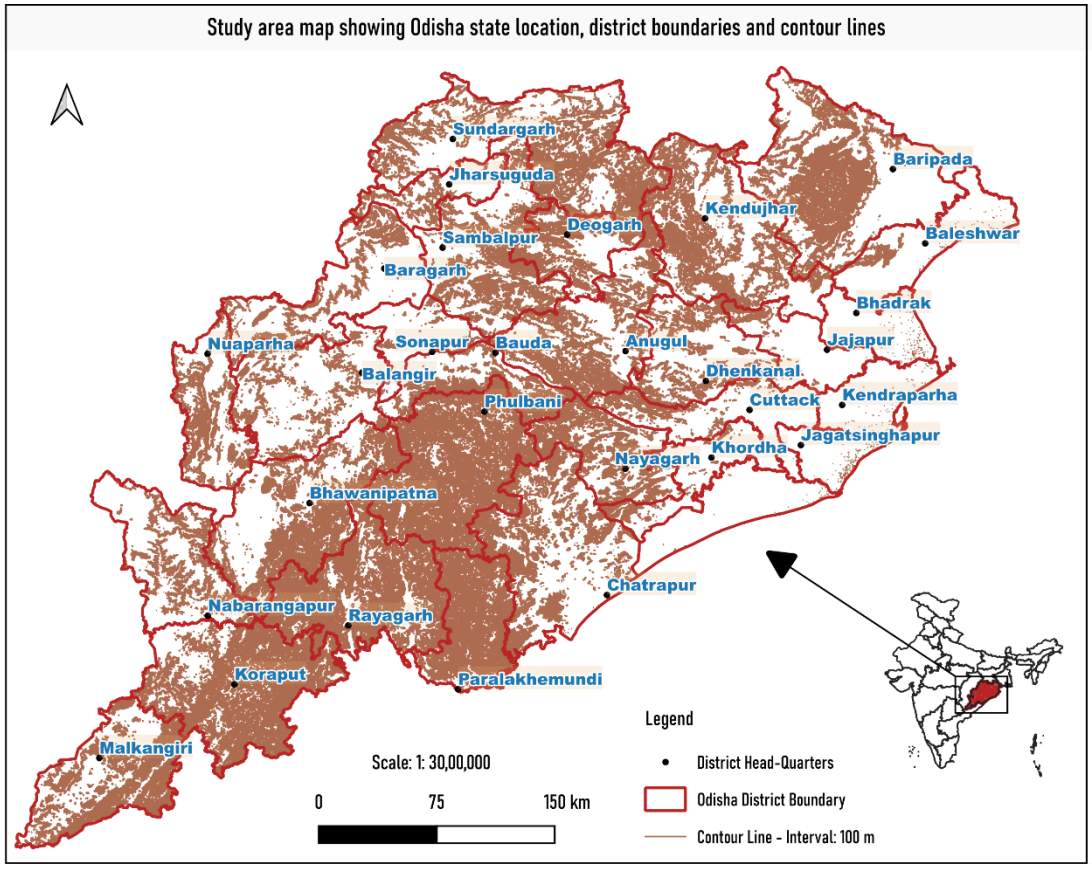

Figure 1: Study area map showing Odisha state location, district boundaries, and contour lines.

https://doi.org/10.5194/egusphere-2025-5269
Preprint. Discussion started: 15 December 2025

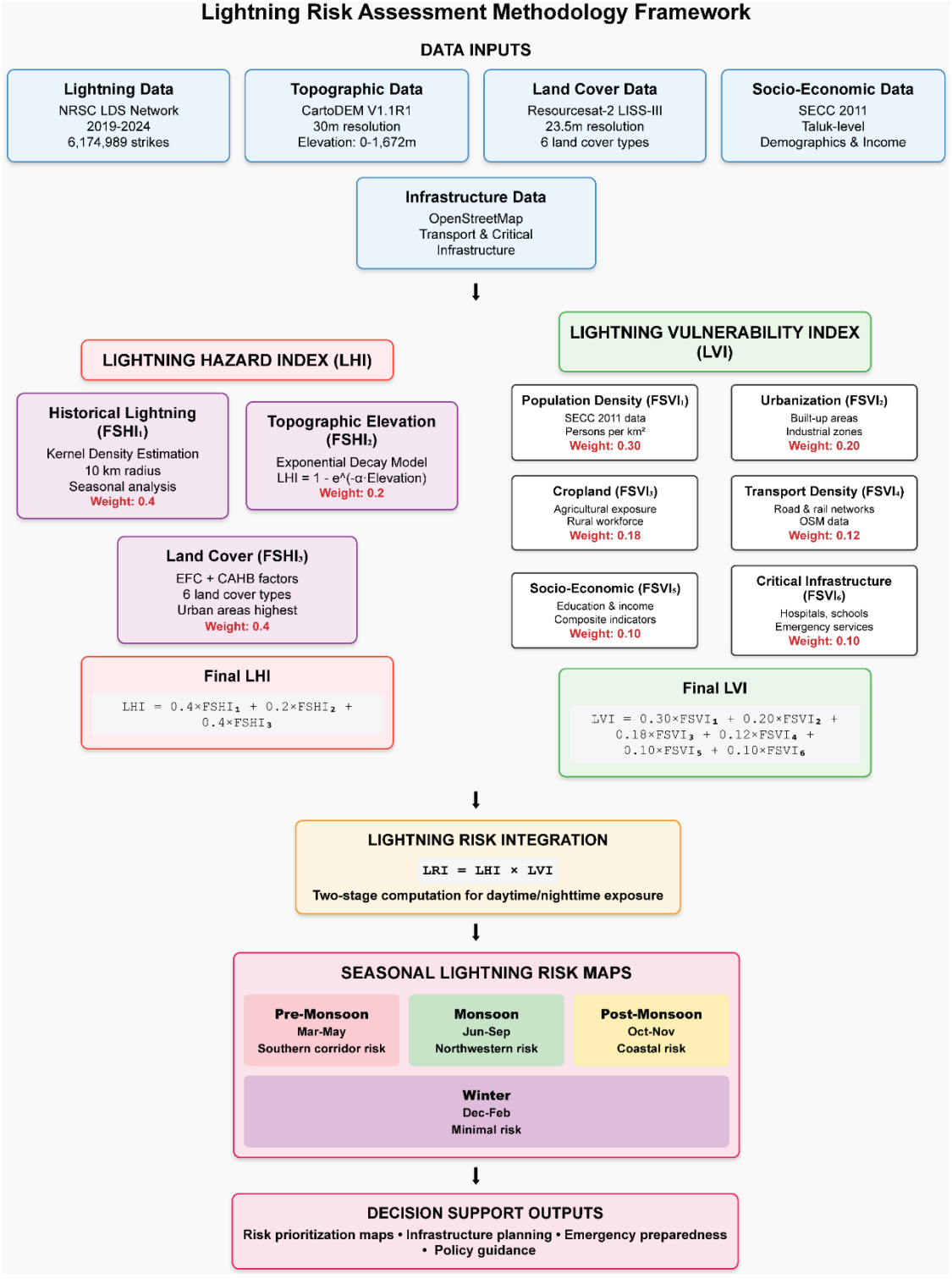

Figure 2: Flowchart showing the integrated lightning risk assessment framework

https://doi.org/10.5194/egusphere-2025-5269
Preprint. Discussion started: 15 December 2025

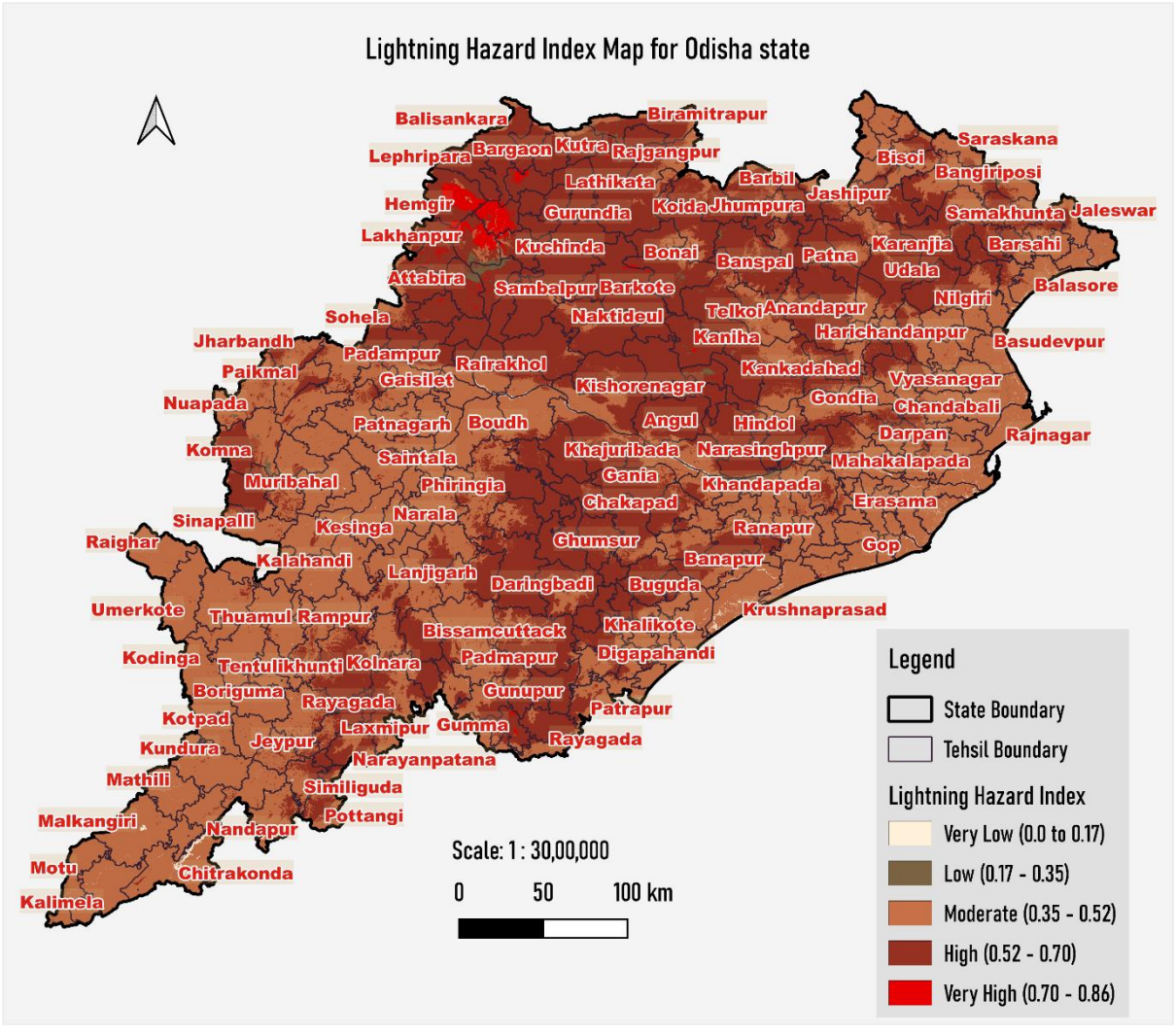

Figure 3: Lightning Hazard Index (LHI) revealing seasonal hazard migration from southern pre-monsoon corridor to northwestern monsoon concentration. Geographic projection: WGS84 UTM Zone 45N.

480

https://doi.org/10.5194/egusphere-2025-5269
Preprint. Discussion started: 15 December 2025

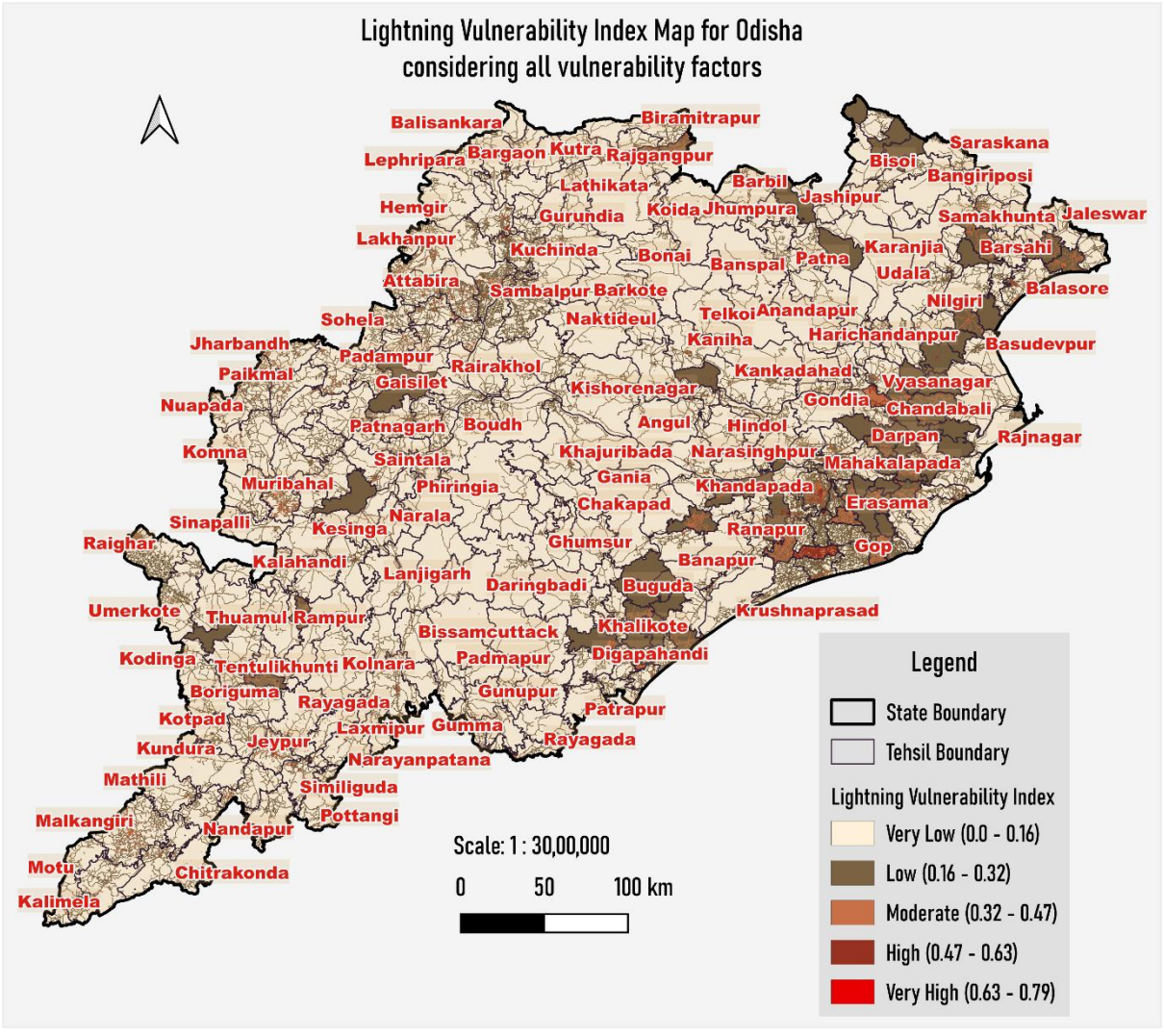

Figure 4: Lightning Vulnerability Index (LVI) demonstrating coastal-urban to tribal-interior gradient with peak vulnerability in eastern coastal tehsils. Geographic projection: WGS84 UTM Zone 45N.

https://doi.org/10.5194/egusphere-2025-5269
Preprint. Discussion started: 15 December 2025

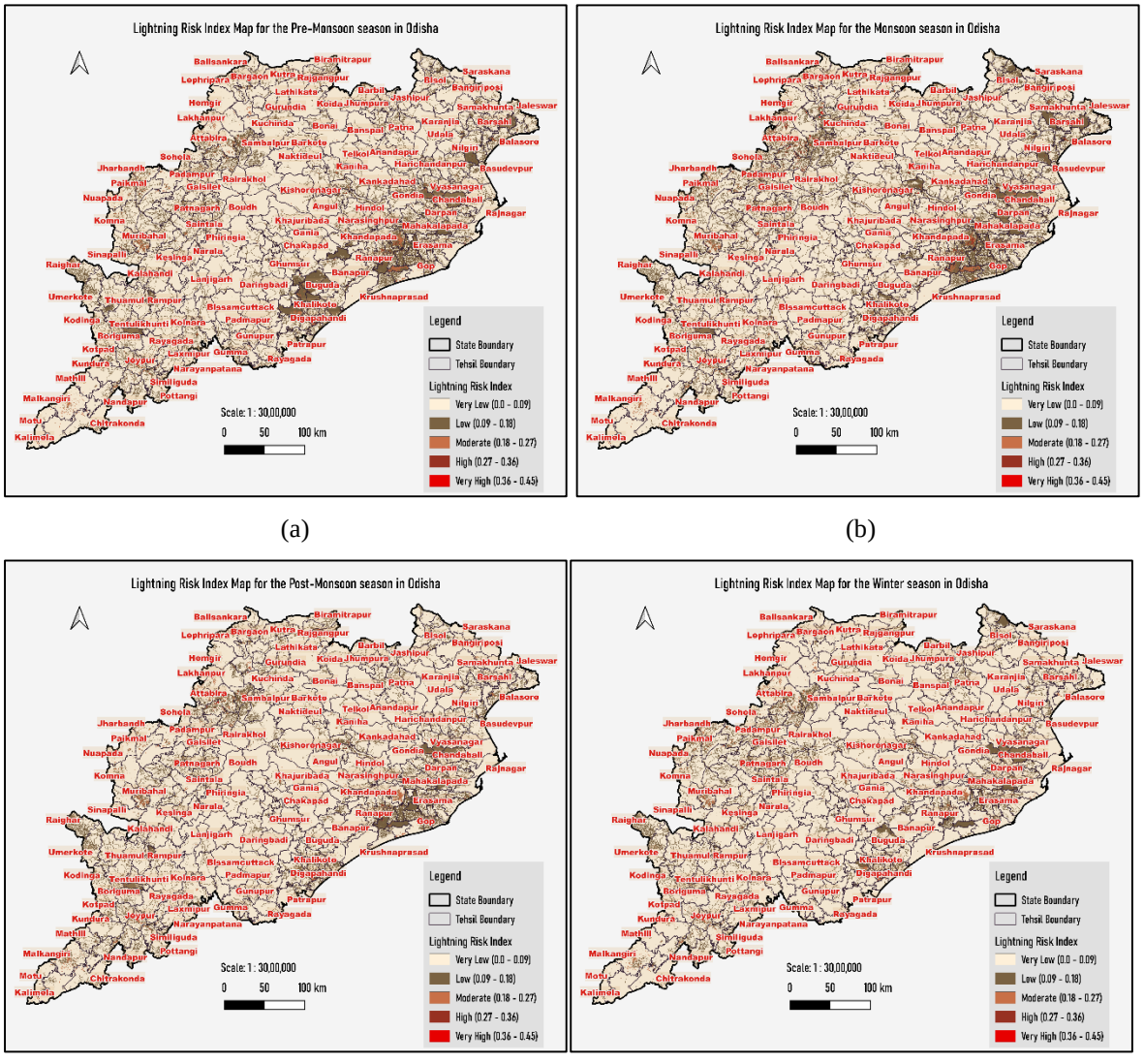

Figure 5: Seasonal Lightning Risk Index (LRI) maps for Odisha showing: (a) Pre-monsoon center-coastal concentration, (b) Monsoon eastern shift, (c) post-monsoon coastal reduction, and (d) Winter minimal risk with central corridor persistence. Maps demonstrate seasonal risk migration patterns for adaptive management strategies.

https://doi.org/10.5194/egusphere-2025-5269
Preprint. Discussion started: 15 December 2025

Land Cover Type	EFC Contribution (%)	CAHB Contribution (%)	Combined $FSHI_3$ Value	Primary Literature Source
Built-up areas	90	60	0.75	*Calin et. al., 2013*
Forest areas	50	70	0.60	*Gora et. al., 2017*
Water bodies	25	85	0.55	*Said et. al., 2013*
Open areas	55	50	0.525	*Rakov & Uman, 2007*

Table 1: Land Cover Lightning Susceptibility Assessment

https://doi.org/10.5194/egusphere-2025-5269
Preprint. Discussion started: 15 December 2025

Mishra et al. (2000–2020) fatality ranking →	Top 20%	20–40%	40–60%	60–80%	Bottom 20%
Mapped "Very High" LRI (this study)	1 (Sundargarh)	1 (Anugul)	2 (Bargarh, Sambalpur)	1 (Jharsuguda)	0
Mapped "High" LRI	2 (Cuttack, Sundargarh)	0	2 (Bargarh, Sambalpur)	1 (Khordha)	0
Mapped "Moderate" LRI	0	1 (Jajapur)	2 (Bargarh, Puri)	1 (Nuaparha)	0
Mapped "Low" LRI	1 (Ganjam)	0	0	0	0
Mapped "Very Low" LRI	0	0	0	0	0

Table 2: Enrichment (LQ > 1) of LRI classes by Mishra fatality quintile (six districts per column; non-exclusive counts; "V" = inclusive OR).

https://doi.org/10.5194/egusphere-2025-5269
Preprint. Discussion started: 15 December 2025

Year	ENSO Phase	Winter	Pre-Monsoon	Monsoon	Post-Monsoon	Annual Total	% of Total
2019	Neutral	50	1,449	165,697	50,238	217,434	**3.5%**
2020	La Niña	3,287	124,567	568,098	73,089	769,041	**12.5%**
2021	La Niña	15,647	341,665	950,816	174,307	1,482,435	**24.0%**
2022	La Niña	14,025	114,878	952,451	101,251	1,182,605	**19.2%**
2023	El Niño	867	518,964	862,501	70,500	1,452,832	**23.5%**
2024	El Niño	5,704	370,797	639,701	54,440	1,070,642	**17.3%**
Total	-	**39,580**	**1,472,320**	**4,139,264**	**523,825**	**6,174,989**	**100.0%**
%	-	**0.6%**	**23.8%**	**67.1%**	**8.5%**	**100.0%**	-

Table 3: Annual and Seasonal Lightning Strike Distribution (2019-2024)